Noninvasive Visualization of Respiratory Viral Infection Using Bioorthogonal Conjugated Near-Infrared-Emitting Quantum Dots

Hong Pan,[†,§] Pengfei Zhang,[†,§] Duyang Gao,[†] Yijuan Zhang,[†] Ping Li,[†] Lanlan Liu,[†] Ce Wang,[†] Hanzhong Wang,[‡] Yifan Ma,[†,*] and Lintao Cai[†,*]

[†]Guangdong Key Laboratory of Nanomedicine, CAS Key Laboratory of Health Informatics, Institute of Biomedicine and Biotechnology, Shenzhen Institutes of Advanced Technology, Chinese Academy of Sciences, Shenzhen 518055, People's Republic of China, and [‡]State Key Laboratory of Virology, Wuhan Institute of Virology, Chinese Academy of Sciences, Wuhan 430071, People's Republic of China. [§]These authors contributed equally to this paper.

ABSTRACT Highly pathogenic avian influenza A viruses are emerging pandemic threats in human beings. Monitoring the *in vivo* dynamics of avian influenza viruses is extremely important for understanding viral pathogenesis and developing antiviral drugs. Although a number of technologies have been applied for tracking viral infection *in vivo*, most of them are laborious with unsatisfactory detection sensitivity. Herein we labeled avian influenza H5N1 pseudotype virus (H5N1p) with near-infrared (NIR)-emitting QDs by bioorthogonal chemistry. The conjugation of QDs onto H5N1p was highly efficient with superior stability both *in vitro* and *in vivo*. Furthermore, QD-labeled H5N1p (QD-H5N1p) demonstrated bright and sustained fluorescent signals in mouse lung tissues, allowing us to visualize respiratory viral infection in a noninvasive and real-time manner. The fluorescence signals of QD-H5N1p in lung were correlated with the severity of virus infection and significantly attenuated by antiviral agents, such as oseltamivir carboxylate and mouse antiserum against H5N1p. The biodistribution of QD-H5N1p in lungs and other organs could be easily quantified by measuring fluorescent signals and cadmium concentration of virus-conjugated QDs in tissues. Hence, virus labeling with NIR QDs provides a simple, reliable, and quantitative strategy for tracking respiratory viral infection and for antiviral drug screening.

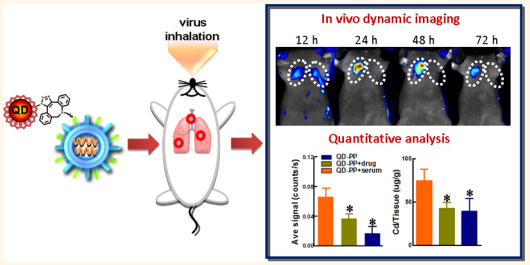

KEYWORDS: bioorthogonal chemistry · near-infrared quantum dots · live virus labeling · viral infection · *in vivo* dynamic imaging

Highly pathogenic avian influenza A viruses are emerging pandemic threats that have caused several outbreaks with high mortality in human beings in the past decades.[1] The infection of avian influenza viruses, such as subtype H5 and H7, could cause a series of severe respiratory and extra-respiratory complications, both of which are directly associated with viral loading and dissemination in tissues.[2] Hence, understanding the route and pathogenesis of avian influenza viral infection is extremely important for developing prophylactic and therapeutic strategies against viral infections. Although the studies using cell cultures have made a significant contribution to exploring the pathogenesis of avian influenza viruses, it is highly desirable to track the *in vivo* dynamics of viral infection in order to further dissect the interactions between the virus and the host.[3,4] The integration of reporter genes, such as fluorescent proteins and luciferase, into viral genomes has been reported as a promising approach for noninvasive virus tracking *in vivo*.[5,6] However, developing genetically engineered viruses requires special expertise and is time-consuming. In addition, the fluorescent imaging of such viruses relies on reporter gene expression, which might limit the detection sensitivity, especially during the early stage of viral infection.[6,7] Virus labeling with organic fluorescent dyes has been recently demonstrated as a promising alternative to track viral invasion *in vitro*.[7] However, the instability and photobleaching of organic dyes potentially limit their application for monitoring virus infection *in vivo*.[8]

* Address correspondence to lt.cai@siat.ac.cn, yf.ma@siat.ac.cn.

Received for review September 28, 2013 and accepted May 5, 2014.

Published online May 05, 2014
10.1021/nn501028b

In the past decade, viral particle labeling with quantum dots (QDs) has emerged as an effective strategy for virus tracking. Compared with conventional fluorescent dyes, QDs demonstrate bright photoluminescence, broad size-tunable emission spectrum, and photochemical stability and have been successfully applied for single-virus tracking *in vitro*.[9−13] Liu *et al.* developed a dual-labeling strategy for single-virus imaging, which labeled the viral envelope and genome with QDs and Syto 82, respectively, and allowed monitoring of both viral particle invasion and viral genome transportation by host cells.[14] Joo *et al.* showed that conjugating QDs to AAV (adeno-associated virus) capsid *via* the carbodiimide chemistry did not affect either the infectivity or the intracellular transport properties of the virus.[15] Unfortunately, it remains a big challenge to use QDs to track viral infection *in vivo*.

An ideal fluorescent labeling for *in vivo* virus tracking must be bright, stable, and capable of penetrating tissues. Recently, QDs with near-infrared (NIR) spectrum from 700 to 900 nm have attracted intense attention due to the ability of deep-tissue imaging in this wavelength range.[8,16−19] NIR QDs have been successfully applied for noninvasive tumor molecular imaging and diagnosis,[20] *in vivo* drug distribution monitoring,[21,22] and lymphatic system imaging.[23] Their application for visualizing viral infection *in vivo*, especially in deep tissues and organs, has not been well-established. Moreover, the stability of QD conjugation is also a critical issue for tracking viral infection *in vivo*. Bioorthogonal chemistry, a biocompatible chemical reaction that can occur in the presence of other rich chemical functionalities found in biological systems without interacting or interfering with native biochemical processes, allowed a wide range of bioactive molecules to be specifically labeled in living organisms.[24−26] Recent studies reported that the copper-free click chemistry was a simple, effective, and bioorthogonal strategy for live viral labeling and did not significantly affect viral infectivity.[27,28]

Avian influenza H5N1 pseudotype virus (H5N1p) has been reported as a safe surrogate of H5N1 virus with similar endocytic pathways and pathological changes as wild-type virus.[29,30] Herein we labeled avian influenza H5N1p with NIR QDs by bioorthogonal reaction[27] and dynamically monitored the respiratory infection of QD-labeled H5N1p (QD-H5N1p) in mice using an *in vivo* imaging system. QD-H5N1p demonstrated bright and sustained fluorescent signals in mouse lung tissues, which were strongly correlated with the severity of viral infection that was verified by lung histology. We also explored the potential application of QD-H5N1p for antiviral drug evaluation. The results showed that the administration of the antiviral agents oseltamivir carboxylate and mouse antiserum significantly affected the *in vivo* dynamics of QD-H5N1p infection, which could be directly quantified by measuring fluorescent signals and cadmium (Cd) concentration of virus-conjugated QDs using inductively coupled plasma/optical emission spectrometry (ICP-OES).

RESULTS AND DISCUSSION

Labeling of H5N1p with NIR QDs *via* Bioorthogonal Chemistry. In the present study, CdSeTe/ZnS alloyed core/shell structured NIR QDs were fabricated using a hot colloidal synthesis approach as previously described.[31,32] The native hydrophobic ligands of QDs were then replaced with multidentate polymer ligands bearing imidazole pendant groups (N_3-PMAH) through ligand exchange to obtain water-dispersible azido-derivatized NIR QD (N_3-QDs) (Supporting Information Figure S1a). The average diameter of N_3-QDs measured by transmission electron microscopy (TEM) was 5.7 nm (see Figure S1b), and the hydrodynamic diameter of the N_3-QDs was ~13.0 nm (Figure S1c). The N_3-QDs had emission wavelength at 750 nm (Figure S1d), and the quantum yield of as-prepared QDs was about 40% (see Methods in the Supporting Information). The results of the MTT assay showed that 1 to 200 μg/mL of N_3-QDs did not significantly affect the viabilities of human lung epithelial A549 cells, murine RAW 264.7 macrophages, and HEK293T cells after 24 h incubation, suggesting the cytotoxicity of N_3-QDs was minimal (Figure S1e).

Bioorthogonal chemistry, which can be conducted under mild conditions, has been reported as an effective method for live virus labeling with QDs.[27,28] We previously established bioorthogonal chemistry for live virus labeling that allowed the specific QD labeling of the viral particle by cycloaddition between the azide moieties on the N_3-QDs and the dibenzocyclooctyl (DBCO) tag on the virus.[27] In the present study, the purified H5N1p was first reacted with DBCO-PEG_4-NHS ester so that DBCO could be effectively conjugated onto the amine group of virus surface proteins. Azide-labeled QDs were then selectively reacted with DBCO-modified H5N1p (DBCO-H5N1p) through the bioorthogonal chemistry to acquire QD-labeled H5N1p (QD-H5N1p) (Figure 1a,c). The hydrodynamic sizes of H5N1p and QD-H5N1p were 100 ± 7.8 and 122 ± 9.7 nm, respectively (Figure 1c). The slight increase of the hydrodynamic size indicated a successful QD conjugation onto the viral particles. Moreover, the bioorthogonal conjugation onto the viral particles did not significantly affect fluorescence intensity or emission spectrum of QDs (Figure 1d).

To determine the optimal dose of N_3-QDs, H5N1p was reacted with different amounts of N_3-QDs at ratios of H5N1p to N_3-QDs from 2.5 to 40 (w/w). The virus-bound and unbound QDs could be separated by the agarose gel electrophoresis due to their different particle sizes.[33] The results showed that when the ratio of H5N1p to N_3-QDs was 20 or above, unbound N_3-QDs were not detectable (Figure 1b), suggesting that QDs were effectively conjugated onto H5N1p. Therefore,

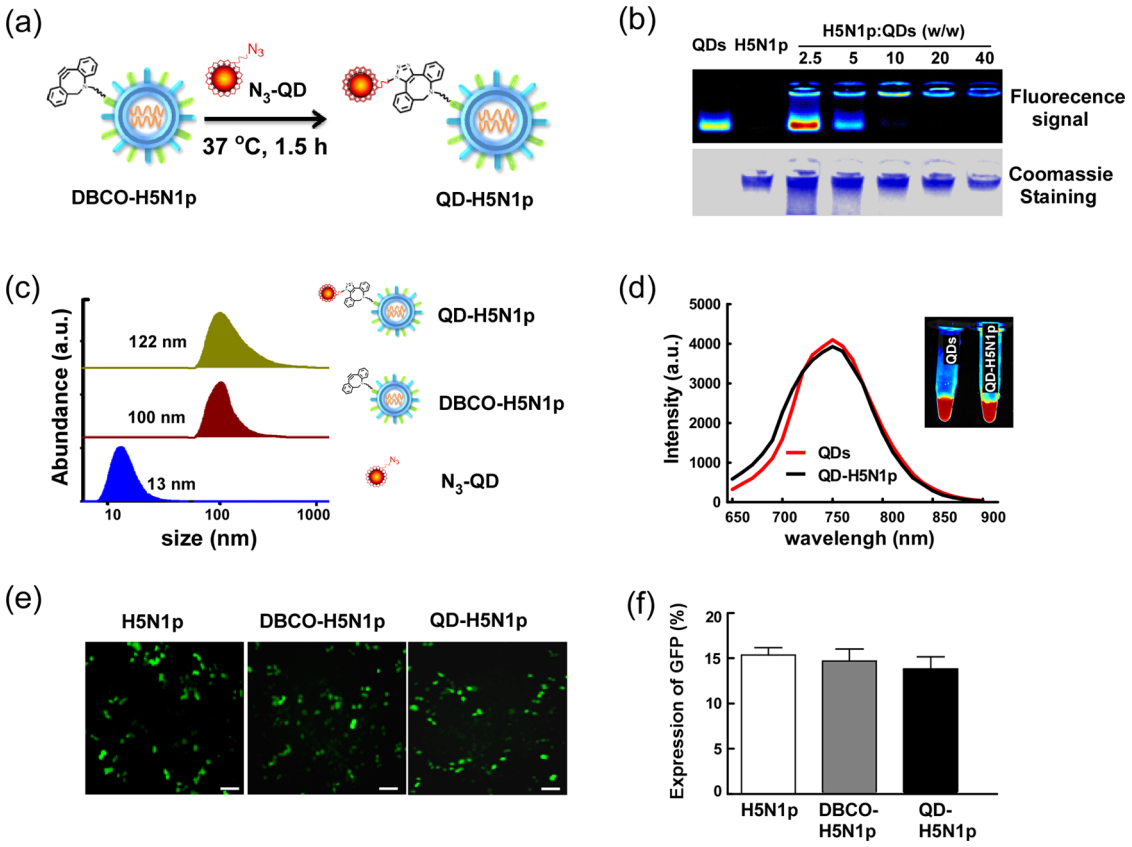

Figure 1. Bioorthogonal labeling of H5N1p with NIR QDs. (a) Schematic illustration of virus labeling with NIR QDs. (b) Agarose gel electrophoresis analysis of H5N1p reacted with different amounts of QDs. The top and bottom panels are the fluorescence image of NIR QDs and Coomassie blue staining of viral particles, respectively. (c) Particle sizes of QDs, H5N1p, and QD-labeled H5N1p (QD-H5N1p). (d) Emission spectrum and fluorescence intensity of QDs and QD-H5N1p. (e,f) Infectivity of H5N1p with or without QD conjugation. HEK293T cells were infected with H5N1p, DBCO-H5N1p, or QD-H5N1p for 24 h, and virus infection was identified by GFP^+ cells using fluorescence microscopy (e). The percentages of GFP^+ cells were quantified by flow cytometry (f). Bars shown are mean ± SE (n = 3–4). Scale bar = 20 μm.

the ratio of H5N1p to N_3-QDs at 20 was applied for future experiments. The infectivity of DBCO-modified H5N1p (DBCO-H5N1p) and QD-H5N1p was evaluated by measuring viral GFP expression in HEK293T cells (Figure 1e). The results showed that neither DBCO modification nor QD conjugation significantly affected viral GFP expression at 24 h post-infection, suggesting that the infectivity of H5N1p was not impaired (Figure 1e,f). Hence, QD labeling with bioorthogonal chemistry is a mild and reliable strategy for live virus labeling.

Stability and Infectivity of QD-H5N1p in A549 Cells. Although QDs have been successfully applied for single-virus tracking in host cells, the stability of QD conjugation remains a big concern. We therefore evaluated the intracellular stability of QD-H5N1p in human lung epithelial A549 cells. A549 cells were incubated with QDs, H5N1p, or QD-H5N1p for 3 h, and the intracellular H5N1p was identified by immunofluorescent staining with the antibody against hemagglutinin (HA), a surface glycoprotein of H5N1. The fluorescent signals of QDs were barely detectable in A549 cells after 3 h incubation with QDs alone, suggesting that the nonspecific internalization of QDs by host cells was minimal. In contrast, both H5N1p and QD-H5N1p were effectively internalized by A549 cells and predominantly distributed in the cytosol at 3 h post-infection, suggesting that QD labeling did not affect either the internalization or intracellular localization of viral particles in A549 cells. More importantly, the green fluorescence of HA was completely colocalized with red fluorescence of NIR QDs, indicating that the viral labeling with QDs by bioorthogonal chemistry was highly efficient. The spectrum of these colocalized dots showed two separated emission peaks at 550 and 750 nm, which could be attributable to the fluorescent dye (Alexa 488) of anti-HA antibody and QDs, respectively (Figure 2a). Hence, the conjugation of QDs to H5N1p was stable in A549 cells upon virus infection (Figure 2a).

Previous studies showed that QDs might not be stable in intracellular compartments, such as lysosomes and peroxisomes.[34] The intracellular biothiols (*e.g.*, glutathione and cysteine) have been shown to degrade the monolayer of QDs, thereby causing QD aggregation and loss of fluorescence.[35] In the present study, H5N1p-conjugated NIR QDs remained detectable with an unshifted fluorescence emission spectrum

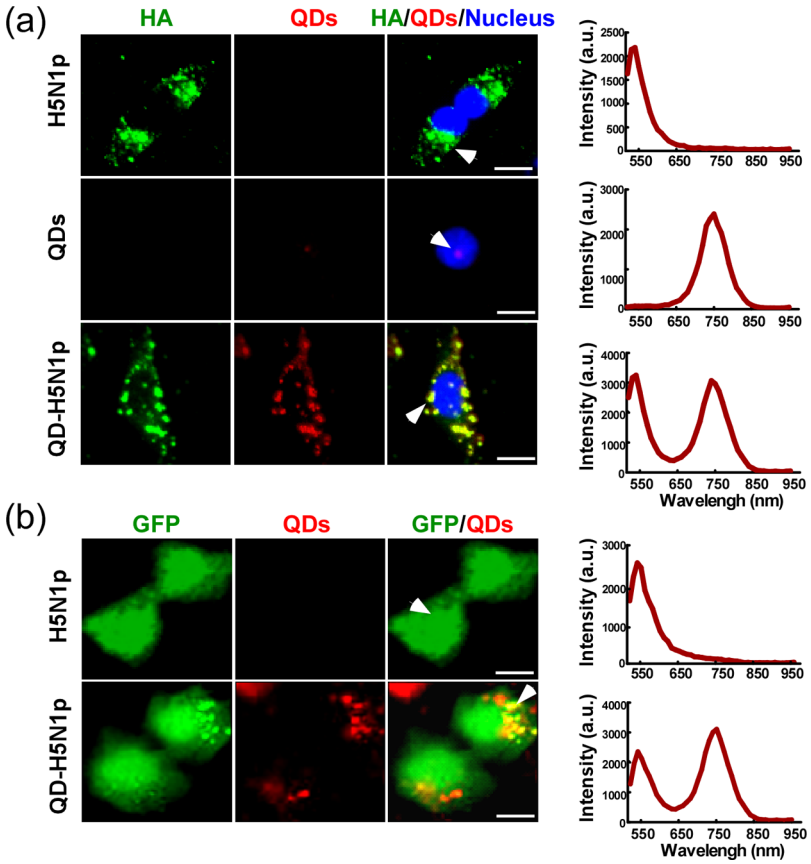

Figure 2. Intracellular localization of QD-H5N1p in A549 cells. A549 cells were treated with H5N1p, QDs, or QD-H5N1p for 3−24 h. (a) Three hours after infection, the cells were labeled with anti-HA antibody, followed by Alexa 488-conjugated anti-IgG (green) to identify viral particles. The fluorescent images of the cells and the spectrum of pointed fluorescent dots were recorded by the multispectral imaging system. Scale bar = 5 μm. (b) Fluorescent images of H5N1p or QD-H5N1p-infected A549 cells and the spectrum of pointed fluorescent dots at 24 h post-infection. Scale bar = 5 μm. Red lines: the fluorescent spectrum.

in virus-infected A549 cells at 24 h after virus infection, indicating their excellent intracellular stability (Figure 2b). The pretreatment of chloroquine (a lysosome inhibitor) did not affect either fluorescence intensity or emission spectrum of virus-conjugated NIR QDs (Figure S2), further suggesting their stability in endosomes and lysosomes. The long-term intracellular stability of QDs might be due to the imidazole-based multidentate polymer ligands of a QD monolayer, which were reported to enhance colloidal stability of nanocrystals more effectively than thiol-based monodendate ligands.[35−37] The bioorthogonal conjugation of NIR QDs to viral particles was highly efficient with remarkable stability in virus-infected cells, which would allow us to monitor the long-term dynamics of viral infection.

***In Vivo* Dynamics of Respiratory Viral Infection in Mice.** To study the *in vivo* dynamics of avian influenza virus infection, Balb/c mice were intranansally (i.n.) infected with live or heat-inactivated QD-H5N1p for 12−72 h, and the fluorescence signal of QDs in lungs was recorded using an *in vivo* imaging system. For comparison, some mice inhaled equal amounts of QDs. The inhalation of QDs resulted in dim and transit fluorescent signals in lungs, which primarily accumulated in the trachea, bronchii, and upper lobes (Figure 3a−c). In contrast, the infection of live QD-H5N1p resulted in bright and sustained fluorescent signals in lungs from 12 to 72 h post-infection with the maximum fluorescence intensity at 24 h. Notably, the fluorescent signals of QD-H5N1p spread to whole lung tissue at 72 h, which should be associated with virus diffusion into lower respiratory tract and pulmonary alveoli.[5] Compared with live QD-H5N1p, the infection of heat-inactivated QD-H5N1p led to dramatically decreased and restricted fluorescent signals in lungs, similar to free QDs did (Figure 3). These data suggested a strong correlation between fluorescent signals of QD-H5N1p and virus infectivity.

To further confirm the conjugation of QDs to H5N1p *in vivo*, lung sections from QD-H5N1p-infected mice were labeled with anti-HA antibody to identify viral particles. Similar to the observation *in vitro*, the immunofluorescent imaging showed nice colocalization of QDs and H5N1 HA in lung epithelium 3 days post-infection. The fluorescence spectrum of the colocalized dots in lung tissues showed two separate emission peaks at 550 and 750 nm, which could be attributable to the fluorescent dye (Alexa 488) of

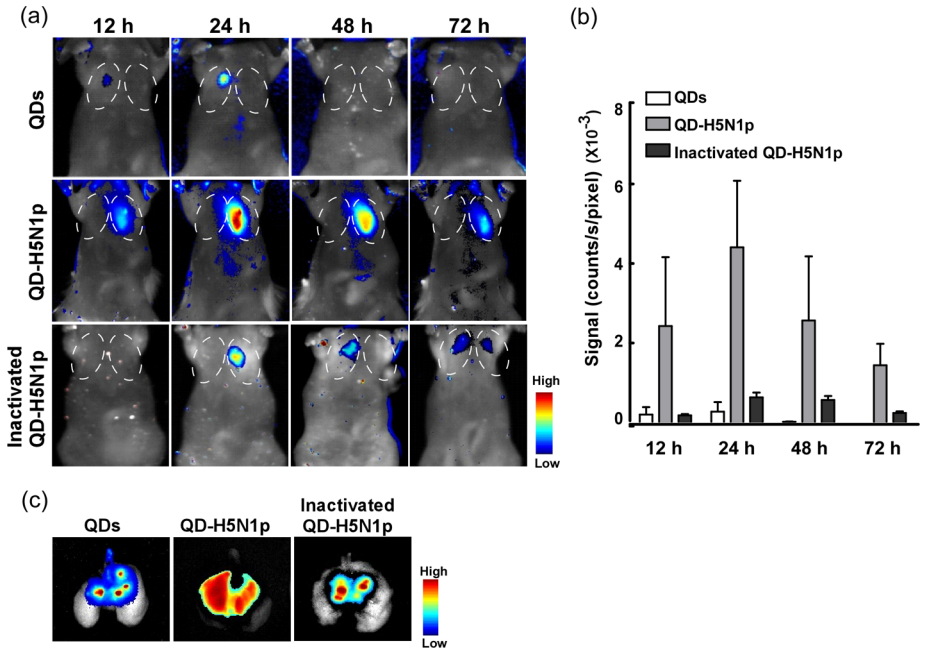

Figure 3. *In vivo* **imaging of respiratory QD-H5N1p infection in mice. Six week old female Balb/c mice were i.n. infected with live or heat-inactivated QD-H5N1p, or with equal amounts of QDs as described in Methods. (a,b) Fluorescent images of mice were recorded at 12−72 h post-infection. The fluorescent signals of circled areas were analyzed using the Maestro software, and the average fluorescence intensity was calculated using the following formula: average signals (counts/s/pixel) = total counts/exposure time (s)/area (pixel). Bars shown are mean ± SE (*n* = 3−4). (c) Fluorescence images of lungs on day 3 post-infection.**

antibodies and QDs as previously observed (Figure 4a,b). These data clearly demonstrated a stable conjugation of NIR QDs to live viruses *in vivo*. Surprisingly, QDs were retained in viral-infected pulmonary epithelium with bright fluorescence and unshifted emission spectrum even on day 6 post-infection (Figure 4c,d). These data indicated the stability of virus-conjugated NIR QDs, which would be essential for long-term tracking of virus infection *in vivo*. The bioorthogonal labeling of NIR QDs could be applied to noninvasively monitor the dynamics of respiratory viral infection in live mice. It is worthy to note that, although the bioorthogonal QD labeling may not be suitable for tracing virus progeny, it allows for the analysis of the route of viral invasion in small animals, which could be important for virology research.

Effect of Antiviral Agents on *In Vivo* Dynamics of Respiratory Viral Infection in Mice. Antiviral drugs and neutralizing antibodies are effective strategies to prevent and treat avian influenza-caused illnesses.[38−40] It is well-known that neuraminidase inhibitors, such as oseltamivir and zanamivir, can prevent the spread of influenza virus by the blocking of viral budding.[38] More recent studies showed that oseltamivir carboxylate (an active form of neuraminidase inhibitors) also inhibited viral entry at the early stage of viral infection.[41−43] Passive immunization with neutralizing antibodies has emerged as another important approach to control influenza virus infection.[44] However, their effect on *in vivo* dynamics of virus infection remains unclear. In the present study, QD-H5N1p was pretreated with oseltamivir carboxylate or mouse antiserum against H5N1p. The pretreatment of oseltamivir carboxylate or antiserum did not significantly affect the fluorescence intensity of QD-H5N1p. The hydrodynamic size of QD-H5N1p was selectively increased by antiserum but not by negative serum (Figure S3). These data suggested antibody-triggered virus aggregation, which is an important mechanism for preventing virus infection.[45] The infectivity of QD-H5N1p with or without pretreatment was evaluated in HEK293T cells. The results showed that the pretreatment of oseltamivir carboxylate or antiserum not only dramatically attenuated the entry of viral particles to HEK293T cells but also diminished the expression of viral GFP by ~50 and ~90%, respectively (Figure S4), confirming their inhibitory effect on virus entry and viral infectivity.[41,45]

The antiviral effect of oseltamivir carboxylate and antiserum was further investigated *in vivo*. The inflammatory response in lung tissues has been reported as a major mechanism contributing to H5N1-caused acute lung injury.[46,47] In the present study, i.n. infection with QD-H5N1p caused significant lung inflammation, including thickening of epithelium and infiltration of inflammatory cells, on day 3 post-infection (Figure 5a,b). The QD-H5N1p significantly increased the mRNA expression of pro-inflammatory cytokines and chemokines, including IL-1β, IL-6, TNFα, and CCL2, in lung tissues (Figure S5). In contrast, the pretreatment of oseltamivir carboxylate or mouse antiserum not only

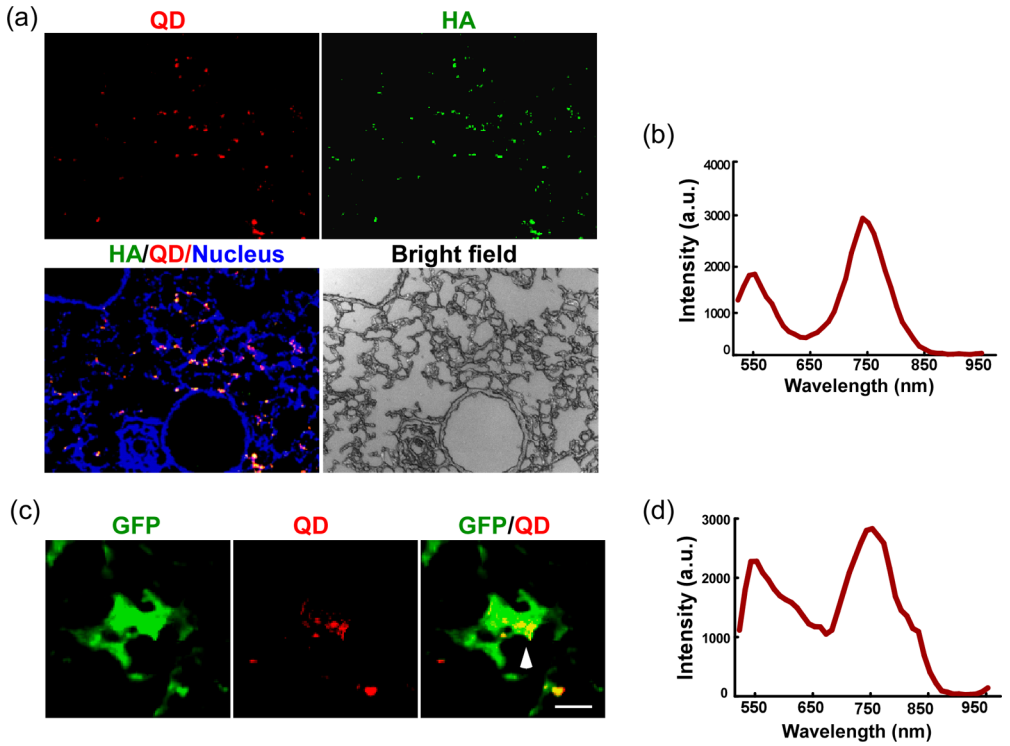

Figure 4. Distribution of QD-H5N1p in lung tissues. (a−e) Three days after infection, lung tissue sections from QD-H5N1p-infected mice were stained with anti-HA antibody and Hoechst to identify viral particles (green) and nuclei (blue), respectively. The fluorescent imaging of lung tissues (a) and the emission spectrum of pointed fluorescent dots (b) were recorded by the multispectral imaging system. Scale bar = 100 μm. (c,d) Fluorescent images of QD-H5N1p-infected pulmonary epithelial cells (GFP^+ cells) were recorded on day 6, and the spectrum of pointed fluorescent dots in the cells was measured as described previously. Scale bar = 20 μm.

attenuated lung pathology caused by virus infection but also reduced mRNA levels of proinflammatory cytokines and chemokines (Figure S5). Hence, both oseltamivir carboxylate and mouse antiserum effectively suppressed respiratory infection of QD-H5N1p in mice.

The effect of antiviral agents on the dynamics of QD-H5N1p infection was further evaluated by the *in vivo* imaging system. Mice were i.n. infected with QD-H5N1p with or without the pretreatment of oseltamivir carboxylate or antiserum, and the fluorescent imaging of mice was recorded from 12 to 72 h post-infection. As we expected, mice infected with untreated QD-H5N1p showed the brightest fluorescence in lung tissues with the maximum fluorescence intensity at 24−48 h (Figure 5c,d). Although oseltamivir carboxylate did not significantly affect the fluorescence intensity of QD-H5N1p, the pretreatment of QD-H5N1p with oseltamivir carboxylate led to 40−60% less fluorescent signals in lungs. Furthermore, QD-H5N1p pretreated with antiserum resulted in the lowest fluorescent signals in lung tissues among three groups (Figure 5c,d). The fluorescence intensity of QD-H5N1p in lungs was nicely correlated with the severity of viral infection, suggesting the bioorthogonal labeling of QDs as a promising strategy for *in vivo* antiviral drug screening. The *ex vivo* analysis of whole lungs showed that the pretreatment of antiviral agents, especially mouse antiserum, lowers fluorescent signals of QD-H5N1p in upper lobes, which should be due to the limited virus spread in lung tissues (Figure 5e). To further determine the distribution of viral particles in lungs, lung sections were labeled with anti-HA antibody. The results showed that the untreated QD-H5N1p was dispersed in the alveolar epithelium, while QD-H5N1p pretreated with antiviral agents mostly accumulated near the main conducting airways with limited diffusion into pulmonary alveoli (Figure S6). These data demonstrated the inhibitory effect of oseltamivir carboxylate and antiserum on virus diffusion in lung tissues, which further confirmed their antiviral effects.

The infection of H5N1 avian influenza has been reported to cause both respiratory and extra-respiratory complications that are directly associated with viral loading and dissemination in the body.[48] Therefore, understanding the biodistribution of viruses *in vivo* is always highly desirable for elucidating the pathology of viral infection. In the present study, since the conjugation of QDs to H5N1p *via* bioorthogonal chemistry demonstrated long-term stability *in vivo*, the distribution of QD-H5N1p in different organs could be easily quantified by measuring the tissue concentration of cadmium, the major element of NIR QDs. The results of ICP-OES showed that the infection of QD-H5N1p led to the highest amount of Cd in lung tissues among three

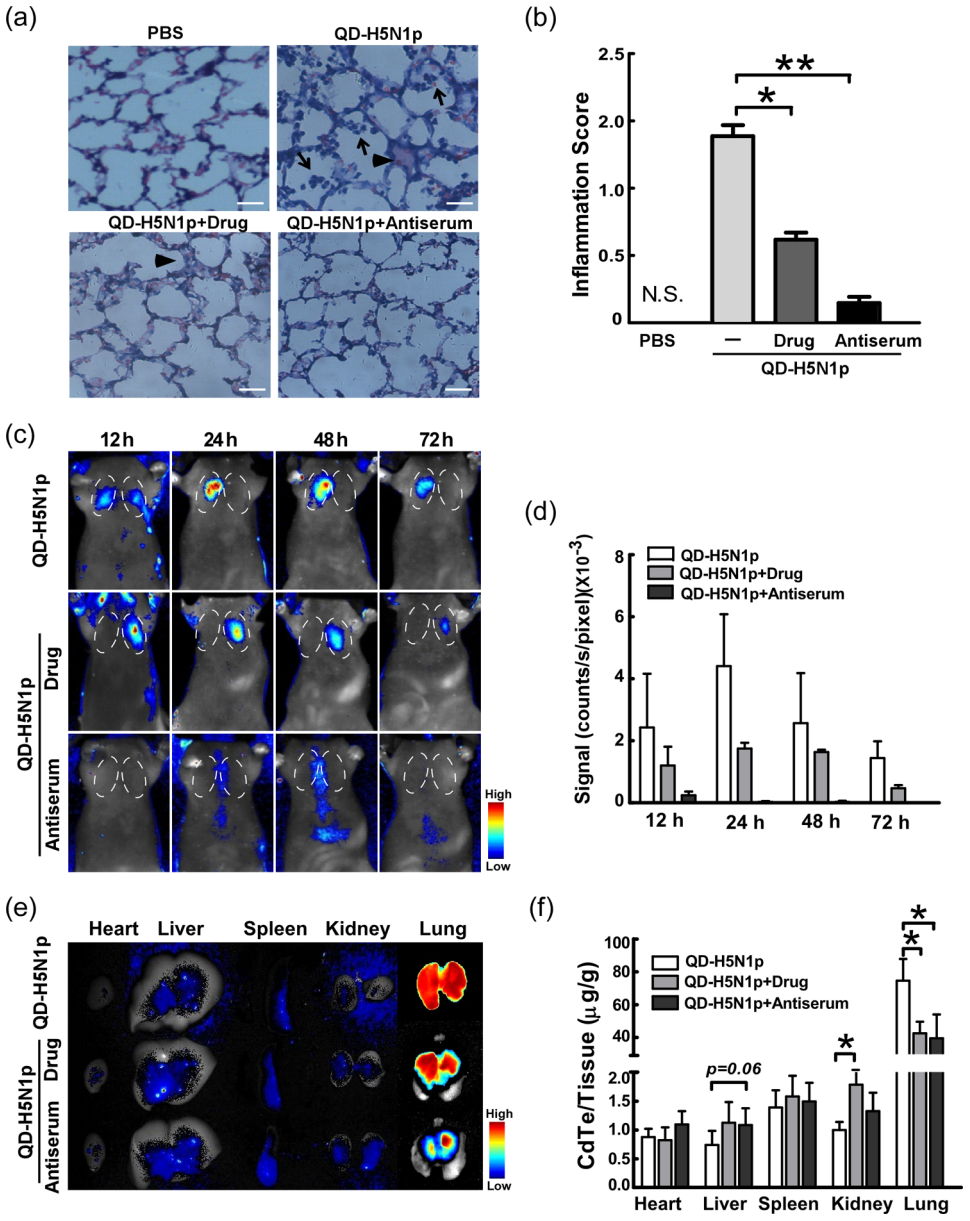

Figure 5. Effect of antiviral agents on the dynamics of respiratory QD-H5N1p infection in mice. Six week old female Balb/c mice were i.n. infected by PBS or QD-H5N1p ± oseltamivir carboxylate (drug) or mouse antiserum against H5N1p (antiserum) as described in Materials and Methods. (a,b) Histopathology of lung tissues on day 3 post-infection was assessed by the H&E staining (a), followed by histopathology scoring (b). (↑) Infiltrated inflammatory cells; (▲) thickening of lung epithelium. Scale bar = 20 μm. (c,d) *In vivo* live imaging of mice at 12−72 h post-infection, and the fluorescent signals of circled regions was quantified as described in Figure 3d. (e) *Ex vivo* fluorescent imaging of hearts, livers, spleens, kidneys, and lungs on day 3 post-infection. (f) ICP-OES analysis of cadmium concentration in different organs 3 days post-infection. Tissue cadmium concentration (μg/g) was calculated by normalizing the amount of cadmium to sample weight. Bars shown are mean ± SE (n = 5), and the differences among groups were determined using one-way ANOVA analysis; *p < 0.05; **p < 0.01.

TABLE 1. Effect of Antiviral Agents on the Biodistribution of QD-H5N1p

	total amount of Cd in organs (% ID[a])				
treatment groups	heart	liver	spleen	lung	kidney
QD-H5N1p	0.30 ± 0.05	3.30 ± 1.11	0.44 ± 0.06	85.69 ± 14.15	1.20 ± 0.14
QD-H5N1p + drug	0.34 ± 0.08	5.87 ± 2.05*	0.43 ± 0.09	54.12 ± 10.2*	2.01 ± 0.25*
QD-H5N1p + antiserum	0.49 ± 0.09	5.84 ± 1.57*	0.43 ± 0.08	53.90 ± 9.49*	1.62 ± 0.39

[a] Cadmium concentration in different organs was measured by ICP-OES analysis on day 3 post-infection, and the percent inoculation dose (% ID) of tissue Cd was calculated using the following formula: % ID = (Cd concentration × organ weight/inoculation dose) × 100%. Data shown are mean ± SE (n = 5), and differences between QD-H5N1p and antiviral agents one-way ANOVA analysis were followed by Tukey' s post-test; *p < 0.05.

groups, while the pretreatment of oseltamivir carboxylate and antiserum dramatically reduced the concentration and total amount of Cd in lungs (Figure 5f and Table 1). These data indicated that antiviral agents significantly reduced the amount of virus loading, the major factor associated with the severity of lung infections,[2] consistent with the result of lung fluorescence imaging. Interestingly, the pretreatment of oseltamivir carboxylate or antiserum increased the amount of Cd in livers and kidneys by 1−2-fold (Table 1), suggesting that the antiviral agents promoted the exit of H5N1p from lungs into blood circulation for excretion.

CONCLUSION

The present study reported virus labeling with bioorthogonal NIR QD conjugation as a simple and reliable strategy for tracking respiratory viral infection *in vivo*. The conjugation of NIR QDs was simple and stable without significantly affecting the infectivity of the virus. Furthermore, virus-conjugated QDs demonstrated bright photoluminescence and photostability and can be imaged in deep tissues, allowing long-term tracing of virus infection in a noninvasive and real-time manner. More importantly, the fluorescence signal of QD-labeled virus in lungs was strongly correlated with the severity of virus infection, and the amount of virus could be quantified by measuring both fluorescent signals and Cd concentration of virus-conjugated QDs in tissues. Hence, live virus labeling with bioorthogonal NIR QDs provides a noninvasive and quantitative tool for monitoring respiratory viral infection and antiviral drug screening.

MATERIALS AND METHODS

Materials. Tellurium powder (Te, 99.8%), selenium shot (Se,99.5%), oleic acid (technical grade, 90%), tri-*n*-octylphosphine oxide (TOPO, 90%), zinc diethyldithiocarbamate (Zn(DDTC)2, 97%), cadmium oxide (CdO, 99.5%), and 1-octadecene (ODE, 90%) were purchased from Strem Chemicals. Oleylamine (OAm, 90%) was from Acros Organics. Poly(maleic anhydride) (MW = 5000 Da) was purchased from PolySciences, Inc., USA. Dibenzocyclooctyne (DBCO-NHS ester) was purchased from Click Chemistry Tools (Scottsdale, AZ). N_3-PEG_8-$CH_2CH_2NH_2$ (MW = 438 Da) was obtained from Biomatrik Inc., China. Unless specified, chemicals were purchased from Sigma-Aldrich (St. Louis, MO) and used without further purification. HEK293T and A549 cells were obtained from Shanghai cell bank of Chinese Academy of Sciences. Oseltamivir acid (ACS: 187227-45-8) was purchased from Shanghai Haoyuan Chemexpress (Shanghai, China). Alexa 488-conjugated goat anti-mouse IgG antibody was from Life technology (NY, USA), and anti-HA protein (H5N1 influenza viruses) mouse monoclonal antibody (mAb) was from Sino Biological Inc. (Beijing, China). Six to eight week old Balb/c mice were obtained from Guangdong Province Laboratory Animal Center (Guangzhou, China) and maintained in the institutional animal care facility. All animal protocols were approved by Institutional Animal Care and Usage Committee of Shenzhen Institutes of Advanced Technology.

Preparation and Characterization of Azido-Derivatized NIR QDs. CdTeSe/ZnS core/shell QDs (em = 750 nm) were prepared as previously reported with slight modification.[31,32] Briefly, 0.56 g of oleic acid, 5 g of TOPO, and 0.26 g of Cd $(OOCCH_3)_2 \cdot 2H_2O$ were heated to 100 °C and degassed for 30 min. The flask was then filled with argon gas, and its temperature was increased to 350 °C. After the precursor Cd was dissolved completely in the solvent, the temperature was decreased to 340 °C and allowed to stabilize for several minutes. At this temperature, premixed Se and Te solution, which was made by dissolving 0.64 g (1 mmol) of Te and 0.4 g in 10 mL of TOP, was quickly injected into the reaction flask. Aliquots of the reaction mixture were taken and quenched in cold chloroform. The as-prepared CdTeSe QDs were isolated through precipitation from excess acetone and then dissolved in hexane. The solution of CdTeSe QDs was diluted in a mixture of trioctylphosphine oxide (5 g) and oleylamine, and hexane was removed under vacuum at 60 °C. The solution was further evacuated for at least 30 min at 100 °C and purged with argon. After being heated to 130 °C, the ZnS shell was grown on the QDs using dropwise injection of a solution of Zn $(DDTC)_2$. The QDs were annealed at 180 °C for 20 min to allow the growth of the ZnS monolayer. When the desired synthesis was completed, the reaction was cooled to room temperature and isolated through precipitation from excess ethanol.

The as-synthesized QD_{750} coated with nonpolar ligands was transferred into aqueous solution by treatment with N_3-PMAH, which was synthesized according to previous published work.[27] The QD solution was mixed with N_3-PMAH solution in DMSO for 10 min, followed by addition of TMAOH to form a biphasic system. After the organic layer was removed, the N_3-PMAH-coated QDs were precipitated by isopropyl alcohol and then resuspended in PBS buffer. Unbound N_3-PMAH ligands were removed by an ultrafiltration device with a cutoff of 50 kDa. The ultraviolet−visible (UV−vis) absorbance spectra and photoluminescence (PL) spectra of QDs were measured using PerkinElmer Lambda 25 UV−vis absorption spectrophotometer and Edinburgh F900 fluorescent spectrometer, respectively. The morphologies of QDs were observed by TEM using a FEI Tecnai G20 transmission microscope at 200 kV. Dynamic light scattering analysis was performed using a Zetasizer Nano ZS (Malvern Instruments).

H5N1p Preparation and Bioorthogonal QD Labeling. H5N1p was prepared in HEK293T cells by transfection with the virus package plasmids as previously described,[49] and viral particles in culture supernatants were purified by ultracentrifugation through a 20% sucrose cushion. The concentration of purified H5N1p was determined using a BCA protein assay kit (Pierce). To determine the titer of H5N1p, HEK293T cells were incubated with serially diluted H5N1p solution for 24 h, and the titer of the virus was calculated with the following formula: clone forming units (CFU)/mL = the number of GFP-positive cells/well × dilution folds.

For viral particle labeling, purified H5N1p was reacted with 0.1 mM DBCO-PEG_4-NHS ester in PBS at 37 °C for 30 min to obtain DBCO-modified H5N1p (DBCO-H5N1p), and unbound DBCO molecules were removed by gel filtration using a NAP-5 desalting column (GE Healthcare). DBCO-H5N1p was then reacted with N_3-PMAH-QD_{750} at different ratios of H5N1p to QDs (w/w) at 37 °C for 1 h to acquire QD-H5N1p.[27] In some experiments, H5N1p was heat-inactivated at 65 °C for 10 min, followed by the bioorthogonal QD labeling. The resulting solution was loaded into a 2% (w/v) agarose gel with Tris-acetate-EDTA (TAE, pH 8.5) running buffer at 80 V for 80 min and visualized using the Maestro *in vivo* imaging system (Cambridge Research & Instrumentation). The viral protein in the agarose gel was stained with Coomassie brilliant blue to ensure equal loading of H5N1p.

Infectivity and Intracellular Localization of QD-H5N1p in Host Cells. HEK293T cells were infected with H5N1p, DBCO-H5N1p, or QD-H5N1p at a multiplicity of infection (MOI) of 0.5 for 48 h, and the infectivity of viral particles was determined by measuring GFP expression using flow cytometry (Becton Dickinson). To investigate the intracellular localization of QD-H5N1p, A549 cells were infected with QD-H5N1p (MOI = 0.5) for 3 to 24 h, followed

by immunofluorescent staining with anti-H5N1 hemagglutinin antibodies (Sino Biological Inc.) and Alexa 488-conjugated donkey anti-rabbit IgG secondary antibodies (Life Technology). The fluorescence image of virus-infected cells was recorded using a Nuance FX multispectral imaging system (PerkinElmer).

Preparation of Mouse Antiserum against H5N1p. Mouse antiserum was prepared as previously described.[49] Briefly, 6 week old female Balb/c mice were subcutaneously immunized by the mixture of H5N1p (20 μg per mouse) in Freund's adjuvant (Sigma) for three times with a 7 day interval, followed by a boost *via* i.v. injection on day 18. Mouse antiserum containing anti-H5N1p antibodies was collected 4 days after the last immunization, and the titer of anti-H5N1p IgG in the antiserum was 1:128000.

Viral Infection Model and *In Vivo* Imaging. Six week old female Balb/c mice were inoculated intranansally with live or heat-inactivated QD-H5N1p (2×10^8 cfu virus and 20 μg QDs per mouse) in 100 μL of PBS buffer. The equal amount of unconjugated QDs was administered as the negative control. In some mice, QD-H5N1p was pretreated with oseltamivir carboxylate (8 μmol/L) or mouse antiserum against H5N1p (1:1000). Virus-infected mice were monitored by CRi Maestro *in vivo* imaging system at 12 to 72 h post-infection. At the end of the experiment, images of heart, lung, liver, spleen, and kidney were recorded by the *in vivo* imaging system, and the average fluorescence intensities were calculated by the following formula: average signals (counts/s/pixel) = total counts/exposure time (s)/area (pixel).

Immunofluorescent Staining and Histopathology of Lung Tissues. Mice were sacrificed on day 3 or day 6 post-infections, and lungs were perfused with 4% paraformaldehyde. The fixed lung tissues were cut into 10 μm sections and labeled with anti-HA antibodies, followed by Alexa 488-conjugated donkey anti-rabbit IgG. The fluorescent images of QDs and H5N1p in lung tissues were recorded using multispectral fluorescence microscopy. To evaluate H5N1p-induced lung inflammation, lung tissue sections were rehydrated in gradient ethanol solutions (from 100 to 75%), followed by staining with hematoxylin and eosin. Lung pathology was assessed by a previously established histopathological scoring system, and 10−20 fields per group were randomly selected for scoring.[50,51]

Quantitative Analysis of NIR QDs by ICP-OES. The amount of QDs in organs was determined by measuring the concentration of Cd using inductively coupled plasmon optical emission spectrometry (ICP-OES) (SPECTRO Analytical Instruments). Weighed tissues were lysed in 68% HNO_3 solution at room temperature overnight, followed by incubation at 70 °C for 1 h. H_2O_2 was then added into each sample until the sample solution became clear. The concentration of cadmium was analyzed by ICP-OES, and the percent inoculation dose (% ID) of tissue Cd was calculated using the following formula: % ID = (Cd concentration × organ weight/inoculation dose) × 100%.

Statistic Analysis. Data were represented as mean ± SEM from at least three independent experiments. The differences among groups were analyzed using paired Student's *t* test or one-way ANOVA analysis followed by Tukey's post-test (Graphpad Prism, GraphPad Software).

Conflict of Interest: The authors declare no competing financial interest.

Acknowledgment. The presented research was financially supported by the National Basic Research Program of China (973 Program No. 2011CB933600), the National Natural Science Foundation of China (81171446, 81071249, 81371679, 20905050), Science and Technology Foundation of Guangdong Province of China (2009A030301010, 2012B090400043, 2012B090600036) and Shenzhen (JC201005270326A, JC201104220242A, JC201005260247A), Guangdong Innovation Research Team of Low-cost Healthcare and SIAT Innovation Program for Excellent Young Researchers (201306).

Supporting Information Available: Supplementary methods and results. This material is available free of charge *via* the Internet at http://pubs.acs.org.

REFERENCES AND NOTES

1. Peiris, J. S.; de Jong, M. D.; Guan, Y. Avian Influenza Virus (H5N1): A Threat to Human Health. *Clin. Microbiol. Rev.* **2007**, *20*, 243–267.
2. de Jong, M. D.; Simmons, C. P.; Thanh, T. T.; Hien, V. M.; Smith, G. J.; Chau, T. N.; Hoang, D. M.; Chau, N. V.; Khanh, T. H.; Dong, V. C.; *et al.* Fatal Outcome of Human Influenza A (H5N1) Is Associated with High Viral Load and Hypercytokinemia. *Nat. Med.* **2006**, *12*, 1203–1207.
3. Saenz, R. A.; Quinlivan, M.; Elton, D.; Macrae, S.; Blunden, A. S.; Mumford, J. A.; Daly, J. M.; Digard, P.; Cullinane, A.; Grenfell, B. T.; *et al.* Dynamics of Influenza Virus Infection and Pathology. *J. Virol.* **2010**, *84*, 3974–3983.
4. Zhang, L.; Guo, Z. W.; Bridge, E. S.; Li, Y. M.; Xiao, X. M. Distribution and Dynamics of Risk Factors Associated with Highly Pathogenic Avian Influenza H5N1. *Epidemiol. Infect.* **2013**, 1–10.
5. Manicassamy, B.; Manicassamy, S.; Belicha-Villanueva, A.; Pisanelli, G.; Pulendran, B.; Garcia-Sastre, A. Analysis of *In Vivo* Dynamics of Influenza Virus Infection in Mice Using a GFP Reporter Virus. *Proc. Natl. Acad. Sci. U.S.A.* **2010**, *107*, 11531–11536.
6. Pan, W.; Dong, Z.; Li, F.; Meng, W.; Feng, L.; Niu, X.; Li, C.; Luo, Q.; Li, Z.; Sun, C.; *et al.* Visualizing Influenza Virus Infection in Living Mice. *Nat. Commun.* **2013**, *4*, 1–8.
7. Hofherr, S. E.; Adams, K. E.; Chen, C. Y.; May, S.; Weaver, E. A.; Barry, M. A. Real-Time Dynamic Imaging of Virus Distribution *in Vivo*. *PLoS One* **2011**, *6*, e17076.
8. Resch-Genger, U.; Grabolle, M.; Cavaliere-Jaricot, S.; Nitschke, R.; Nann, T. Quantum Dots *versus* Organic Dyes as Fluorescent Labels. *Nat. Methods* **2008**, *5*, 763–775.
9. Zhang, Y.; Ke, X.; Zheng, Z.; Zhang, C.; Zhang, Z.; Zhang, F.; Hu, Q.; He, Z.; Wang, H. Encapsulating Quantum Dots into Enveloped Virus in Living Cells for Tracking Virus Infection. *ACS Nano* **2013**, *7*, 3896–3904.
10. Joo, K.-I.; Lei, Y.; Lee, C.-L.; Lo, J.; Xie, J.; Hamm-Alvarez, S. F.; Wang, P. Site-Specific Labeling of Enveloped Viruses with Quantum Dots for Single Virus Tracking. *ACS Nano* **2008**, *2*, 1553–1562.
11. Bentzen, E. L.; House, F.; Utley, T. J.; Crowe, J. E.; Wright, D. W. Progression of Respiratory Syncytial Virus Infection Monitored by Fluorescent Quantum Dot Probes. *Nano Lett.* **2005**, *5*, 591–595.
12. Liu, S. L.; Zhang, Z. L.; Tian, Z. Q.; Zhao, H. S.; Liu, H.; Sun, E. Z.; Xiao, G. F.; Zhang, W.; Wang, H. Z.; Pang, D. W. Effectively and Efficiently Dissecting the Infection of Influenza Virus by Quantum-Dot-Based Single-Particle Tracking. *ACS Nano* **2012**, *6*, 141–150.
13. Cui, Z. Q.; Ren, Q.; Wei, H. P.; Chen, Z.; Deng, J. Y.; Zhang, Z. P.; Zhang, X. E. Quantum Dot−Aptamer Nanoprobes for Recognizing and Labeling Influenza A Virus Particles. *Nanoscale* **2011**, *3*, 2454–2457.
14. Liu, S. L.; Tian, Z. Q.; Zhang, Z. L.; Wu, Q. M.; Zhao, H. S.; Ren, B.; Pang, D. W. High-Efficiency Dual Labeling of Influenza Virus for Single-Virus Imaging. *Biomaterials* **2012**, *33*, 7828–7833.
15. Joo, K. I.; Fang, Y.; Liu, Y.; Xiao, L.; Gu, Z.; Tai, A.; Lee, C. L.; Tang, Y.; Wang, P. Enhanced Real-Time Monitoring of Adeno-Associated Virus Trafficking by Virus-Quantum Dot Conjugates. *ACS Nano* **2011**, *5*, 3523–3535.
16. Yang, K.; Zhang, F. J.; Tang, H.; Zhao, C.; Cao, Y. A.; Lv, X. Q.; Chen, D.; Li, Y. D. *In-Vivo* Imaging of Oral Squamous Cell Carcinoma by EGFR Monoclonal Antibody Conjugated Near-Infrared Quantum Dots in Mice. *Int. J. Nanomed.* **2011**, *6*, 1739–1745.
17. Baker, M. Nanotechnology Imaging Probes: Smaller and More Stable. *Nat. Methods* **2010**, *7*, 957–962.
18. Allen, P. M.; Liu, W.; Chauhan, V. P.; Lee, J.; Ting, A. Y.; Fukumura, D.; Jain, R. K.; Bawendi, M. G. InAs(ZnCdS) Quantum Dots Optimized for Biological Imaging in the Near-Infrared. *J. Am. Chem. Soc.* **2009**, *132*, 470–471.
19. Zhang, Y.; Hong, G.; Zhang, Y.; Chen, G.; Li, F.; Dai, H.; Wang, Q. Ag_2S Quantum Dot: A Bright and Biocompatible Fluorescent Nanoprobe in the Second Near-Infrared Window. *ACS Nano* **2012**, *6*, 3695–3702.

20. Gao, J.; Chen, K.; Luong, R.; Bouley, D. M.; Mao, H.; Qiao, T.; Gambhir, S. S.; Cheng, Z. A Novel Clinically Translatable Fluorescent Nanoparticle for Targeted Molecular Imaging of Tumors in Living Subjects. *Nano Lett.* **2012**, *12*, 281–286.
21. Nehilla, B. J.; Allen, P. G.; Desai, T. A. Surfactant-Free, Drug-Quantum-Dot Coloaded Poly(lactide-*co*-glycolide) Nanoparticles: Towards Multifunctional Nanoparticles. *ACS Nano* **2008**, *2*, 538–544.
22. Yezhelyev, M. V.; Qi, L.; O'Regan, R. M.; Nie, S.; Gao, X. Proton-Sponge Coated Quantum Dots for siRNA Delivery and Intracellular Imaging. *J. Am. Chem. Soc.* **2008**, *130*, 9006–9012.
23. Bhang, S. H.; Won, N.; Lee, T. J.; Jin, H.; Nam, J.; Park, J.; Chung, H.; Park, H. S.; Sung, Y. E.; Hahn, S. K.; *et al.* Hyaluronic Acid–Quantum Dot Conjugates for *In Vivo* Lymphatic Vessel Imaging. *ACS Nano* **2009**, *3*, 1389–1398.
24. Sletten, E. M.; Bertozzi, C. R. Bioorthogonal Chemistry: Fishing for Selectivity in a Sea of Functionality. *Angew. Chem., Int. Ed.* **2009**, *48*, 6974–6998.
25. Algar, W. R.; Prasuhn, D. E.; Stewart, M. H.; Jennings, T. L.; Blanco-Canosa, J. B.; Dawson, P. E.; Medintz, I. L. The Controlled Display of Biomolecules on Nanoparticles: A Challenge Suited to Bioorthogonal Chemistry. *Bioconjugate Chem.* **2011**, *22*, 825–858.
26. Best, M. D. Click Chemistry and Bioorthogonal Reactions: Unprecedented Selectivity in the Labeling of Biological Molecules. *Biochemistry* **2009**, *48*, 6571–6584.
27. Zhang, P.; Liu, S.; Gao, D.; Hu, D.; Gong, P.; Sheng, Z.; Deng, J.; Ma, Y.; Cai, L. Click-functionalized Compact Quantum Dots Protected by Multidentate-Imidazole Ligands: Conjugation-Ready Nanotags for Living-Virus Labeling and Imaging. *J. Am. Chem. Soc.* **2012**, *134*, 8388–8391.
28. Hao, J.; Huang, L.-L.; Zhang, R.; Wang, H.-Z.; Xie, H.-Y. A Mild and Reliable Method To Label Enveloped Virus with Quantum Dots by Copper-Free Click Chemistry. *Anal. Chem.* **2012**, *84*, 8364–8370.
29. Pan, H.; Zhang, Y.; Luo, Z.; Li, P.; Liu, L.; Wang, C.; Wang, H.; Li, H.; Ma, Y. Autophagy Mediates Avian Influenza H5N1 Pseudotyped Particle-Induced Lung Inflammation through NF-κB and p38 MAPK Signaling Pathways. *Am. J. Physiol.: Lung Cell. Mol. Physiol.* **2014**, *6*, L183–195.
30. Garcia, J. M.; Lai, J. C. Production of Influenza Pseudotyped Lentiviral Particles and Their Use in Influenza Research and Diagnosis: An Update. *Expert Rev. Anti-Infect. Ther.* **2011**, *9*, 443–455.
31. Pons, T.; Lequeux, N.; Mahler, B.; Sasnouski, S.; Fragola, A.; Dubertret, B. Synthesis of Near-Infrared-Emitting, Water-Soluble CdTeSe/CdZnS Core/Shell Quantum Dots. *Chem. Mater.* **2009**, *21*, 1418–1424.
32. Hu, D.; Zhang, P.; Gong, P.; Lian, S.; Lu, Y.; Gao, D.; Cai, L. A Fast Synthesis of Near-Infrared Emitting CdTe/CdSe Quantum Dots with Small Hydrodynamic Diameter for *In Vivo* Imaging Probes. *Nanoscale* **2011**, *3*, 4724–4732.
33. Bucking, W.; Massadeh, S.; Merkulov, A.; Xu, S.; Nann, T. Electrophoretic Properties of BSA-Coated Quantum Dots. *Anal. Bioanal. Chem.* **2010**, *396*, 1087–1094.
34. Muro, E.; Fragola, A.; Pons, T.; Lequeux, N.; Ioannou, A.; Skourides, P.; Dubertret, B. Comparing Intracellular Stability and Targeting of Sulfobetaine Quantum Dots with Other Surface Chemistries in Live Cells. *Small* **2012**, *8*, 1029–1037.
35. Zhu, Z. J.; Yeh, Y. C.; Tang, R.; Yan, B.; Tamayo, J.; Vachet, R. W.; Rotello, V. M. Stability of Quantum Dots in Live Cells. *Nat. Chem.* **2011**, *3*, 963–968.
36. Stewart, M. H.; Susumu, K.; Mei, B. C.; Medintz, I. L.; Delehanty, J. B.; Blanco-Canosa, J. B.; Dawson, P. E.; Mattoussi, H. Multidentate Poly(ethylene glycol) Ligands Provide Colloidal Stability to Semiconductor and Metallic Nanocrystals in Extreme Conditions. *J. Am. Chem. Soc.* **2010**, *132*, 9804–9813.
37. Liu, W.; Greytak, A. B.; Lee, J.; Wong, C. R.; Park, J.; Marshall, L. F.; Jiang, W.; Curtin, P. N.; Ting, A. Y.; Nocera, D. G.; *et al.* Compact Biocompatible Quantum Dots *via* RAFT-Mediated Synthesis of Imidazole-Based Random Copolymer Ligand. *J. Am. Chem. Soc.* **2010**, *132*, 472–483.
38. De Clercq, E. Antiviral Agents Active Against Influenza A Viruses. *Nat. Rev. Drug Discovery* **2006**, *5*, 1015–1025.
39. Yu, X. C.; Tsibane, T.; McGraw, P. A.; House, F. S.; Keefer, C. J.; Hicar, M. D.; Tumpey, T. M.; Pappas, C.; Perrone, L. A.; Martinez, O.; *et al.* Neutralizing Antibodies Derived from the B Cells of 1918 Influenza Pandemic Survivors. *Nature* **2008**, *455*, 532–536.
40. Du, L.; Li, Y.; Zhao, G.; Wang, L.; Zou, P.; Lu, L.; Zhou, Y.; Jiang, S. Highly Pathogenic Avian Influenza A(H5N1) Mutants Transmissible by Air Are Susceptible to Human and Animal Neutralizing Antibodies. *Int. J. Infect. Dis.* **2013**, *208*, 1315–1319.
41. Ohuchi, M.; Asaoka, N.; Sakai, T.; Ohuchi, R. Roles of Neuraminidase in the Initial Stage of Influenza Virus Infection. *Microbes Infect.* **2006**, *8*, 1287–1293.
42. Gao, R. B.; Du, N.; Liu, D. S.; Li, Z.; Zhu, Y.; Shu, Y. L. Oseltamivir Inhibits Both Viral Entry and Release but Enhances Apoptosis of Cells Infected with Influenza A H1N1. *Biochem. Biophys. Res. Commun.* **2013**, *431*, 788–795.
43. Matrosovich, M. N.; Matrosovich, T. Y.; Gray, T.; Roberts, N. A.; Klenk, H. D. Neuraminidase Is Important for the Initiation of Influenza Virus Infection in Human Airway Epithelium. *J. Virol.* **2004**, *78*, 12665–12667.
44. Dilillo, D. J.; Tan, G. S.; Palese, P.; Ravetch, J. V. Broadly Neutralizing Hemagglutinin Stalk-Specific Antibodies Require Fc gamma Interactions for Protection Against Influenza Virus *in Vivo*. *Nat. Med.* **2014**, *20*, 143–1451.
45. Marasco, W. A.; Sui, J. The Growth and Potential of Human Antiviral Monoclonal Antibody Therapeutics. *Nat. Biotechnol.* **2007**, *25*, 1421–1434.
46. Guan, Y.; Poon, L. L.; Cheung, C. Y.; Ellis, T. M.; Lim, W.; Lipatov, A. S.; Chan, K. H.; Sturm-Ramirez, K. M.; Cheung, C. L.; Leung, Y. H.; *et al.* H5N1 Influenza: A Protean Pandemic Threat. *Proc. Natl. Acad. Sci. U.S.A.* **2004**, *101*, 8156–8161.
47. Simmons, C.; Farrar, J. Insights into Inflammation and Influenza. *N. Engl. J. Med.* **2008**, *359*, 1621–1623.
48. Korteweg, C.; Gu, J. Pathology, Molecular Biology, and Pathogenesis of Avian Influenza A (H5N1) Infection in Humans. *Am. J. Pathol.* **2008**, *172*, 1155–1170.
49. Tao, L.; Chen, J.; Zheng, Z.; Meng, J.; Zhang, Z.; Chen, Y.; Luo, H.; Li, H.; Chen, Z.; Hu, Q.; *et al.* H5N1 Influenza Virus-like Particles Produced by Transient Expression in Mammalian Cells Induce Humoral and Cellular Immune Responses in Mice. *Can. J. Microbiol.* **2012**, *58*, 391–401.
50. Buchweitz, J. P.; Karmaus, P. W.; Harkema, J. R.; Williams, K. J.; Kaminski, N. E. Modulation of Airway Responses to Influenza A/PR/8/34 by Δ9-Tetrahydrocannabinol in C57BL/6 Mice. *J. Pharmacol. Exp. Ther.* **2007**, *323*, 675–683.
51. Wang, J.; Li, F.; Sun, R.; Gao, X.; Wei, H.; Li, L. J.; Tian, Z. Bacterial Colonization Dampens Influenza-Mediated Acute Lung Injury *via* Induction of M2 Alveolar Macrophages. *Nat. Commun.* **2013**, *4*, 1–10.